Complex multidisciplinary optimization of turbine blading systems

P. LAMPART[1], Ł. HIRT[2]

[1] *The Szewalski Institute of Fluid Flow Machinery*
Polish Academy of Sciences in Gdańsk
Fiszera 14
80-231 Gdańsk, Poland
e-mail: lampart@imp.gda.pl

[2] *The Faculty of Ship Building and Ocean Engineering*
Technical University of Gdańsk
Narutowicza 11/12
80-233 Gdańsk, Poland
e-mail: lukasz.hirt@pg.gda.pl

THE PAPER DESCRIBES the methods and results of direct optimization of turbine blading systems using a software package Opti_turb. The final shape of the blading is obtained from minimizing the objective function, which is the total energy loss of the stage, including the leaving energy. The current values of the objective function are found from 3D RANS computations (from a code FlowER) of geometries changed during the process of optimization. There are constraints imposed on the mass flow rate, exit swirl angle and reactions, as well as on changes of stresses in the metal.

Among the optimized parameters are those of the blade itself (such as the blade number and stagger angle as well as the stacking blade line parameters) and those of the blade section (profile). Two new hybrid stochastic-deterministic methods are used for the optimization of flow systems. The first method is a combination of a genetic algorithm and a simplex method of Nelder–Mead. The other method is a combination of a direct search method of Hooke–Jeeves and simulated annealing. Also two methods of parametrization of the blade profile are described. They make use of a set of circle arcs and Bezier functions.

In the course of optimization, the flow efficiency of a group of two low pressure (LP) exit stages of a 50 MW turbine operating over a wide range of load is increased by means of optimization of 3D blade stacking lines. Another practical example of efficiency optimization of turbine blading systems is modification of low load profiles PLK-R2 for high pressure (HP) steam turbine stages. It is shown that optimization of geometry of turbine blading systems can give considerable efficiency gains. Optimization of 3D blade stacking lines in LP turbine stages can give over a 2% efficiency rise. Up to 1% efficiency, increase can be obtained from optimization of HP blade profiles and their restaggering.

Key words: optimization, steam turbines, flow systems, CFD, RANS model .

1. Introduction

The efficiency of turbine stages can be increased by optimization of blading systems, including classical optimization of stator and rotor blade numbers and stagger angles, as well as optimization of blade sections (profiles) and 3D blade stacking lines. The possible large number of shape parameters of 3D turbine blading requires efficient optimization techniques.

The effects of blade reprofiling and 3D blade stacking are generally known. Change of the blade profile redistributes profile load and changes the state of boundary layers at the blade suction surface, thus changing the distribution of profile loss. The redistribution of profile load (making the profile front-loaded or aft-loaded) also has an effect of redistribution of endwall/secondary flow losses [1]. 3D blade stacking redistributes span-wise blade load, mass flow rate, changes the state of boundary layers at the blade suction surface and at the endwalls, and can serve as a means of controlling endwall/secondary flow and tip leakage losses [2–5]. By 3D blade stacking it is also possible to reduce span-wise variations of the exit velocity and swirl angle, which is likely to reduce downstream mixing losses and make stator/rotor matching easier. The quantitative effect of blade reprofiling and 3D blade stacking on the overall loss coefficient of the turbine stage depends on the way of reprofiling and blade stacking, and varies with turbine stage geometry and operational conditions. The largest efficiency gains obtained from reblading are usually achieved in low pressure (LP) turbines, which is shown in [6, 7].

There are two main approaches to optimization of turbomachinery blading systems. One approach concentrates on development of 3D inverse design using Euler or Navier–Stokes codes, where the shape of the blading changes during iterative procedures so as to reach the target distribution of, for example, blade surface static pressure or static pressure difference [8, 9]. Another approach focuses on optimization of global characteristics of the stage and the final shape is obtained from minimizing an objective function, for example the total enthalpy of total pressure loss of the turbine stage. Values of the objective function for new geometries can be found directly from 3D viscous flow computations [6, 7].

The largest costs during efficiency optimization of flow systems are connected with the calculation of values of the objective function (flow losses of the changing flow system), which are usually obtained from a RANS solver. Therefore, approximate models to calculate the objective function such as an artificial neural network trained over a data base of high-fidelity 3D RANS solutions are often used [10, 11]. Among new optimization strategies are surrogate model accelerated multi-objective evolutionary algorithms [12]. Particularly popular and effective are Kriging and especially co-Kriging methods, where the response surface models of the high-fidelity function are constructed from a combination of

expensive high-fidelity and other cheap low-fidelity data [13]. New direct optimization methods are also devised to choose new geometries in the optimization process and to be effective both for single-extremum and multimodal objective functions. Among these new methods are hybrid stochastic-deterministic algorithms described in [14–16].

In this paper, we describe two new stochastic-deterministic optimization methods used in the code Opti_turb. The first method is a combination of a genetic algorithm and simplex method of Nelder–Mead. The other method is a combination of a direct search method of Hooke–Jeeves and simulated annealing. Also two methods of parametrization of the blade profile are described. They make use of a set of circle arcs and Bezier functions. As shown in the paper, these methods allow efficient optimization of turbomachinery blading systems.

2. Optimization of turbomachinery blading systems

2.1. Objective function

Optimization is an iterative procedure that seeks for an extremum of the objective function

$$\min_x f(\mathbf{y}(\mathbf{x}), \mathbf{x}) \quad \text{or} \quad \max_x f(\mathbf{y}(\mathbf{x}), \mathbf{x})$$

assuming that $y \in [y_{\min}; y_{\max}]$, $x \in [x_{\min}; x_{\max}]$, where f is an objective function, $\mathbf{y}$ – vector of the assumed flow parameters, $\mathbf{x}$ – vector of the assumed geometrical parameters. In the code Opti_turb, the objective function is built based on the flow loss coefficient. It is just the enthalpy loss of the turbine stage (stage group) for a single-point optimization:

$$f = \xi,$$

where ξ is the enthalpy loss including the exit energy (definitions of enthalpy losses in blade rows and stages are included in the Appendix). For turbines operating over a wide range of load, the optimum geometry is found from a multipoint optimization procedure, where the objective function is a weighted average of objectives for a number of selected flow regimes

$$f = \sum_{k=1,n} w^{(k)} \xi^{(k)}, \qquad \text{where} \qquad \sum_{k=1,n} w^{(k)} = 1.$$

In order to simultaneously improve the aerodynamic performance, heat transfer processes as well as mechanical and thermal integrity of the blading, multidisciplinary optimization can also be switched on. An objective function is defined then to gather information from different solvers representing each involved discipline and to assure the required coupling between the disciplines.

2.2. Shape parameters

The following parameters of blade shape can be considered during the optimization for each blade row:

— blade number and stagger angle,
— blade height,
— blade linear lean angle, linear sweep angle and linear twist angle,
— compound lean parameters Δx, Δy (2 at hub, 2 at tip),
— compound sweep parameters Δx, Δy (2 at hub, 2 at tip),
— compound twist parameters Δx, Δy (2 at hub, 2 at tip),
— a number of blade profile parameters.

As compared to the blade with the originally straight stacking line, the blade obtained in the process of optimization can be linearly or non-linearly leaned in the circumferential direction and swept in the axial direction. The blade can also be linearly or non-linearly twisted about its stacking line. The idea of compound lean or sweep, their parametrization by the parabolic functions and the corresponding shape parameters are explained in the Appendix, whereas the next subsection is concerned with the description of the applied methods of parametrization of the blade profile.

2.3. Parametrization of blade profile

Two methods of parametrization of the blade profile are included in the code Opti_turb to facilitate shape optimization of the blade profile. They make use of the set of circle arcs and Bezier functions.

Circle arcs

The idea of blade profile description by means of circle arcs is well-known. Several groups of stator and rotor profiles, such as N1-N3, PLK and R1-R3 profiles, are just built based on the set of 3 to 7 circle arcs on the pressure and suction surface of the profile, [17]. Each arc is determined by its circle centre coordinates and radius, see Fig. 1. Subsequent arcs remain tangent to each other,
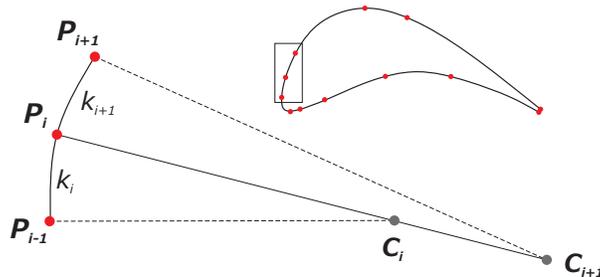

Fig. 1. Blade profile parametrization using circle arcs.

which makes the pressure and suction surface of the profile smooth. The pressure and suction surface are linked by two more circle arcs which form the leading and trailing edge of the profile. In the course of optimization, the distribution of circle arcs and their parameters is varied. The tangency condition implies that the tangency point P_i and the neighbouring circles' centres c_{1i}, c_{i+1} lie on the same line.

Bezier curves

The idea of approximation of blade profiles by means of Bezier functions and samples of blade profile optimization based on this approximation was presented in [11]. In this work, we make use of a special form of Bezier functions, that is a rational Bezier function [18].

The rational Bezier curve is a parametric curve described by the following formula:

$$Q(t) = \frac{\sum_{i=0,n} w_i B_{i,n}(t) P_i}{\sum_{i=0,n} w_i B_{i,n}(t)},$$

where: $t \in \langle 0, 1 \rangle$, P_i – control point given by coordinates $\{x_i, y_i\}$, w_i – weight for control point P_i, $B_{i,n}$ – Bernstein polynomial given by

$$B_{i,n} = \binom{n}{i} t^i (1-t)^{n-i}.$$

The shape of a Bezier curve is affected by its control points and their weights. For a 3rd order Bezier function ($n=3$) each curve is defined by 4 control points – 2 end points and 2 internal points, Fig. 2. A weight is prescribed to each
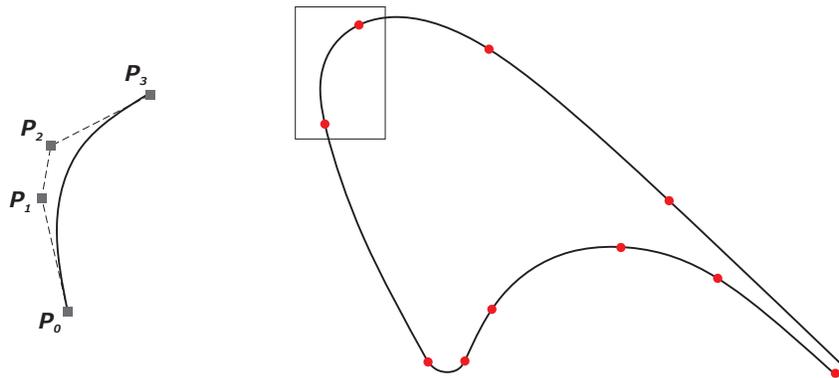

FIG. 2. The blade profile approximation with rational Bezier curves; P_0, P_3 – end control points, P_1, P_2 – internal control points.
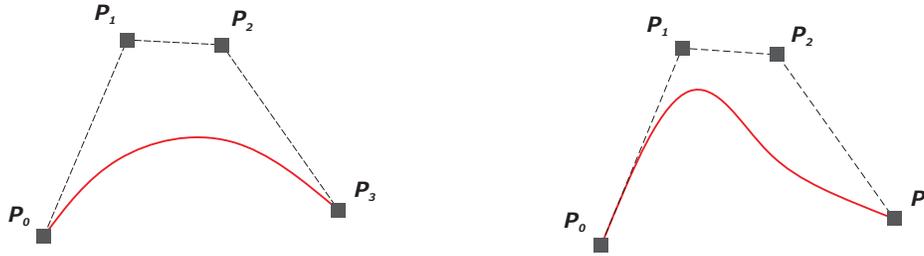
FIG. 3. The effect of weight change on the shape of a rational Bezier curve; original curve –
all weights are set to unity (left), modified curve – the weight corresponding to point P_1 is
increased (right).

control point. Fig. 3 exhibits the effect of sample weights' change on the shape
of a rational Bezier curve. Subsequent Bezier curves are assumed to be tangent
to each other to make the pressure and suction surface of the profile smooth.
During the optimization, the shape of the profile is varied by varying Bezier
curves and their parameters.

2.4. Optimization constraints

Optimization of blading systems should be conducted as constrained opti-
mization. Constraints refer both to geometric parameters, which are the opti-
mized parameters, as well as to flow and structure parameters, which are not
directly optimized so as to assure that they do not fall beyond the allowed range
of variation. The following sample flow/structure parameters can be considered
during optimization: exit flow angle, mean reaction, reaction at the root and tip,
mass flow rate and stresses in the metal.

Geometric and flow parameters to be controlled during optimization are con-
strained in two ways. Stiff constraints are used with respect to the exit angle,
reactions and stresses in the metal, meaning that the objective function acquires
a certain large value if the allowed range of variation of these parameters is
exceeded:

$f = \xi$ if the parameters fall within the allowed range of variation,

$f = \infty$ otherwise or if flow calculations do not converge,

where ξ is a value of the objective function (enthalpy loss coefficient) obtained
from CFD computations.

Beside stiff constraints, weak constraints are also considered during the op-
timization process. In this type of constraint, usually applied to the mass flow
rate (resultant for a flow solver assuming the pressure drop across the stage
as a boundary condition – see the next subsection), a penalty is assigned to
the objective function if a flow characteristic falls beyond the required interval
$[G_-, G_+]$ around a design value of flow rate G:

$$f = \xi \qquad\qquad\qquad \text{if } G_- \leq G \leq G_+,$$
$$f = \xi + \min[(G - G_\pm)^2]/\varepsilon \quad \text{otherwise,}$$

where ε is the penalty coefficient, usually prescribed in a way that the objective function sharply rises to infinity with the increasing distance from the limits of the assumed range of variation. As the pressure drop during optimization is kept constant and the mass flow rate is constrained in a very narrow range of variation, any change of power of the optimised stage is due to the reduced flow losses only.

The above formula used during single-point optimization is modified for the case of multi-point optimization

$$f = \sum_{k=1,n} w^{(k)}\xi^{(k)} \quad \text{if for each } k G_-^{(k)} \leq G_-^{(k)} \leq G_+^{(k)},$$

$$f = \sum_{k=1,n} w^{(k)}\xi^{(k)} + \max_k(\min[(G^{(k)} - G_\pm^{(k)})^2])/\varepsilon \quad \text{otherwise,}$$

where $G^{(k)}$ is the current mass flow rate calculated at a point (load) k and $[G_-^{(k)}, G_+^{(k)}]$ is the allowed narrow interval of flow rate change around the design value at this point (load) k.

2.5. Flow and structure solvers

Flow computations of turbomachinery geometries are made with the help of a computer code FlowER [19, 20], where turbulent flow of compressible viscous gas is described by 3D RANS equations with the perfect gas equation. Turbulence effects are modeled using the k-ω SST (shear stress transport) model [21]. This two-equation eddy-viscosity model (blend of k-ω in the near-wall region and k-ε in the wake region) has been proved to be successful in 2D and 3D test computations of flows over bodies and aerodynamic surfaces, giving the right rate of production and dissipation of turbulent kinetic energy in boundary layers, wakes and separation regions. Discretization of governing equations is made by the finite volume method. A numerical scheme of second-order accuracy in time and space is used. This is an upwind scheme of Godunov type with an ENO formula for the calculation of convective fluxes. To accelerate the process of convergence, an implicit operator δ of Beam–Warming is used.

The calculations are carried out in one blade-to-blade passage of the stator and rotor on an H-type grid refined near the endwalls, blade walls ($y^+ = 1$–2), leading and trailing edges. Typically, 12–16 points are used in the boundary layer. The total number of grid points per one blade-to-blade passage (of a single blade row) exceeds 400 000 (92 axially $\times$ 76 radially $\times$ 60 circumferentially). The calculations converge to a steady state. A mixing plane approach is used to treat the relative motion of the stator and rotor, based on circumferential

averaging of flow parameters in the axial gaps between the blade rows. The calculation domain also extends on the radial gaps above the unshrouded rotor blades (tip leakage region). The assumed boundary conditions are typical for turbomachinery calculations, including no slip and zero heat flux at the walls, as well as spatial periodicity at the borders of the flow channel. The pressure drop across the stage (stage group) is imposed. Therefore, for a given flow geometry, the mass flow rate is resultant.

The assumed structure solver WYKA [22, 23] was originally elaborated for numerical analysis of deformations of marine propellers. It is based on finite elements of medium-thickness shells – eight-node isoparametric elements whose shape functions are second-order polynomials. The solver enables the static analysis of main and reduced stresses, calculation of frequencies and modes of natural vibrations as well as enables the calculation of deformations and wear analysis of material subject to unsteady load. By means of an interface system it is integrated with the flow solver and optimization package [24].

2.6. Direct optimization or neural network

The largest costs during efficiency optimization of flow systems are connected with the calculation of values of the objective function (flow losses of the changing flow system calculated from a RANS solver). Due to time restrictions, RANS computations in the course of optimization are carried out on coarse grids, also using faster and less expensive turbulence models. After optimization, the original and optimized geometries are recalculated on refined grids. In validation of the optimization results, more advanced turbulence models available in the code ANSYS Fluent [25] can also be used. As shown in [26], Reynolds stress models, such as the LRR model [27], can provide additional insight to the development of secondary flows. Intermittency γ based models [28] can improve the prediction of transitional flows.

One way to speed up the optimization procedure is to use approximate models to calculate the objective function such as an artificial neural network trained over a data base of RANS solutions. In the code Opti_turb, the back-propagation method is used to train the neural network (in the MATLAB environment) [24]. New direct optimization methods are also devised to choose new geometries in the optimization process and to be effective both for single-extremum and multimodal objective functions.

2.7. Deterministic or stochastic optimization methods

Typical deterministic methods of optimization such as the direct search method of HOOKE–JEEVES [29] and the simplex method of NELDER–MEAD [30] are effective for objective functions having a single extremum. However, they may

not be effective in the case of multimodal functions having a number of extrema as they tend to reduce the range of search and hold on to a local extremum. Stochastic methods such as genetic algorithms [31] and simulated annealing [32] are very reliable in finding global extrema of multimodal functions. Unfortunately, the stochastic methods clearly exhibit a low rate of convergence in the vicinity of the extremum, which largely increases computational costs of optimization. A solution may be the application of hybrid stochastic-deterministic schemes [14–16].

2.8. Genetic algorithm with a simplex

This hybrid method starts with a genetic algorithm so as to approach the vicinity of the global extremum. The real coding with the modified selection, cross-over and mutation operators are used. The initial population is found in the process of evenly random generation within the search domain. To reduce the computational costs, two worst elements are removed from the population after each iteration. Typical entry data for the genetic algorithm are:

n – number of parameters (dimension of the objective function),
$\mathbf{x}_{i,\min}$, $\mathbf{x}_{i,\max}$ – lower and upper boundaries of the search region,
$Npop = 50$–200 – population,
$P_k = 0.8$–0.9 – cross-over probability,
$P_m = 0.01$–0.02 – mutation probability,
$RanGen$ – model of random number generator,
M – maximum number of iterations.

After a prescribed number of iterations, the best point is selected and an initial simplex for the Nelder–Mead method is built around it. Typical entry data for the Nelder–Mead method are:

n – number of dimensions,
$\mathbf{x}^{(0)}$, L_{simp} – initial point and width of the regular simplex,
α, γ, β, σ – reflection, expansion, contraction and reduction coefficient,
ε – termination criterion.

The effectiveness of this hybrid method was first tested on a chained Rosenbrock (banana-valley) function and on a multimodal trigonometric function [31], typical test functions used for testing optimization algorithms. The n-dimensional Rosenbrock function has a form:

$$F(x_1, x_2, \ldots, x_n) = \sum_{i=2}^{n} [100(x_{i-1}^2 - x_i^2) + (x_{i-1}^2 - 1)^2], \qquad n - \text{even number.}$$

This function has a single extremum $F = 0$ at a point $(1, 1, \ldots, 1)$. A standard difficult starting point of the optimization algorithm for this function is e.g. $x_0 = (x_i)$, $x_{2i-1} = -1.2$, $x_{2i} = 1.0$.

The chosen trigonometric function has the form:

$$F(x_1, x_2, \ldots, x_n) = 0.025 \sum_{i=1}^{n} (x_i - x_{\min})^2$$
$$+ \sin^2\Big(\sum_{i=1}^{n}(x_i - x_{\min}) + \sum_{i=1}^{n}(x_i - x_{\min})^2\Big) + \sin^2\Big(\sum_{i=1}^{n}(x_i - x_{\min})\Big).$$

The trigonometric function contains an infinite number of local minima and one global minimum $F = 0$ at $(x_{\min}, x_{\min}, x_{\min}, \ldots, x_{\min})$. Assuming $x_{\min} = 1$ implies that the global minimum is located at $(1, 1, \ldots, 1)$. A standard starting point for the optimization algorithm for this function is also chosen as: $x_0 = (x_i)$, $x_{2i-1} = -1.2$, $x_{2i} = 1.0$

Typical results of searching for the extremum of the chained Rosenbrock function (for $n = 8$) using the hybrid genetic algorithm/simplex method, are shown in Tab. 1. Here, after 7 iterations of the genetic algorithm (above 1000

Table 1. Searching for the extremum of the chained Rosenbrock function ($n = 8$) using the genetic algorithm/Nelder–Mead method; $Npop = 150$, $P_k = 0.8$, $P_m = 0.01/\alpha = 1$, $\gamma = 2$, $\beta = 0.5$, $\sigma = 0.5$.

GA

ITER	NUM_F	F	X[1]	X[2]	X[3]	X[4]
1	150	0.481304E+003	−0.703430E+000	0.108514E+001	−0.408735E+000	0.251600E−001
3	448	0.216897E+003	0.109331E+001	0.634627E+000	0.126386E+000	0.922287E+000
5	738	0.120122E+003	0.106995E+001	0.581012E+000	0.331034E+000	0.890497E+000
7	1020	0.601066E+002	0.103055E+001	0.736448E+000	0.761536E+000	0.110106E+001

ITER	X[5]	X[6]	X[7]	X[8]
1	−0.666257E+000	0.651096E+000	0.384433E+000	0.130870E+001
3	0.504271E+000	0.556767E+000	0.104408E+001	0.650910E+000
5	0.676535E+000	0.359990E+000	0.612750E+000	0.438051E+000
7	0.106005E+001	0.116355E+001	0.124722E+001	0.118540E+001

NM

ITER	NUM_F	F	X[1]	X[2]	X[3]	X[4]
1	9	0.601066E+002	0.103055E+001	0.736448E+000	0.761536E+000	0.110106E+001
50	84	0.172511E+002	0.985756E+000	0.831754E+000	0.843429E+000	0.973664E+000
105	175	0.961207E+000	0.952637E+000	0.951463E+000	0.957433E+000	0.157723E+001
170	270	0.100508E+001	0.977154E+000	0.976662E+000	0.976375E+000	0.625150E+000
200	317	0.100282E+001	0.100347E+001	0.993324E+000	0.990686E+000	0.607854E-001

ITER	X[5]	X[6]	X[7]	X[8]
1	0.106005E+001	0.116355E+001	0.124722E+001	0.118540E+001
50	0.942047E+000	0.108663E+001	0.126807E+001	0.149645E+001
105	0.100713E+001	0.105729E+001	0.111670E+001	0.125121E+001
170	0.100639E+001	0.102702E+001	0.102121E+001	0.104471E+001
200	0.997619E+000	0.999060E+000	0.992528E+000	0.975497E+000

calculations of the function) and 200 iterations of the Nelder–Mead method (above 300 calculations of the function), the function value can be reduced by 4 orders of magnitude. In Table 2, the case of the trigonometric function (for $n = 10$) is illustrated. Here, after 4 iterations of the genetic algorithm (below 800 calculations of the function) and 200 iterations of the Nelder–Mead method (350 calculations of the function), the function is also reduced by 4 orders of magnitude. The subsequent columns of the presented tables give the number of iterations (ITER), number of calculations of the objective function (NUM_F), value of the objective function (F) and values of the coordinates (X[I]).

Table 2. Searching for the global extremum of the trigonometric function ($n = 10$) using the genetic algorithm/Nelder-Mead method; $\textbf{\textit{Npop}} = 200$, $P_k = 0.8$, $P_m = 0.01/\alpha = 1$, $\gamma = 2$, $\beta = 0.5$, $\sigma = 0.5$.

GA

ITER	NUM_F	F	X[1]	X[2]	X[3]	X[4]
1	200	0.131903E+001	0.145763E+001	0.101102E+001	0.144413E+001	0.133822E+001
2	400	0.904608E+000	0.202245E+000	0.182581E+001	0.171015E+001	0.183924E+001
3	598	0.757878E+000	0.486811E+000	0.110099E+001	0.835161E+000	0.788966E+000
4	794	0.463378E+000	0.155080E+001	0.722796E+000	0.102589E+001	0.754722E+000

ITER	X[5]	X[6]	X[7]	X[8]	X[9]	X[10]
1	0.745425E+000	0.199738E+001	0.105864E+001	0.498509E+000	0.187955E+001	0.196547E+001
2	0.117716E+001	0.864176E+000	0.122678E+001	0.114751E+001	0.165614E+001	0.124589E+001
3	0.139465E+001	0.475123E+000	0.393143E+000	0.117504E+001	-0.273289E+000	0.614738E+000
4	0.485169E+000	0.895392E+000	0.920030E+000	0.997540E+000	0.116690E+001	0.107523E+001

NM

ITER	NUM_F	F	X[1]	X[2]	X[3]	X[4]
1	11	0.463378E+000	0.155080E+001	0.722796E+000	0.102589E+001	0.754722E+000
49	110	0.122838E-001	0.102242E+001	0.107326E+001	0.996109E+000	0.978358E+000
78	163	0.105178E-002	0.980918E+000	0.104317E+001	0.100193E+001	0.998394E+000
125	231	0.109636E-003	0.100460E+001	0.100474E+001	0.999193E+000	0.996552E+000
200	350	0.327654E-004	0.100527E+001	0.100057E+001	0.100187E+001	0.999157E+000

ITER	X[5]	X[6]	X[7]	X[8]	X[9]	X[10]
1	0.485169E+000	0.895392E+000	0.920030E+000	0.997540E+000	0.116690E+001	0.107523E+001
49	0.965412E+000	0.104298E+001	0.972888E+000	0.100484E+001	0.101457E+001	0.993391E+000
78	0.988238E+000	0.101788E+001	0.101687E+001	0.995948E+000	0.985121E+000	0.969062E+000
125	0.996993E+000	0.999189E+000	0.100198E+001	0.100994E+001	0.100232E+001	0.988345E+000
200	0.100183E+001	0.999751E+000	0.998781E+000	0.100105E+001	0.100157E+001	0.990621E+000

2.9. Simulated annealing Hooke–Jeeves method

This hybrid scheme is a modification of the Hooke–Jeeves method, which includes elements of classical simulated annealing. Similar to the original Hooke–Jeeves scheme, two stages of calculations can be distinguished: trial and working stage.

In the trial stage, the vicinity of a base point is searched along all directions of the ortogonal coordinate system. If the trial stage is successful, in the working step the old base point is moved to a new base point.

If not, the Metropolis test is performed. A random number r is generated from the interval [0,1] and compared with $p = \exp(-\delta f/T)$, where δf is a local increase of the objective function, T is the control parameter called temperature. If $r < p$ then the best point obtained in the trial step is accepted as a new base point. The random factor thus introduced enables the algorithm to go beyond the local extremum. The scheme requires a careful definition of the temperature.

The entry data for this hybrid algorithm are:

n – number of parameters (dimension of the objective function),
$\mathbf{x}^0$ – starting point,
τ – initial step length,
$\alpha = 0.8$ – step reduction coefficient,
T – temperature,
ε – termination criterion.

Typical results of searching for the global extremum of the chained Rosenbrock function and trigonometric function (for $n = 10$) using the Hooke–Jeeves/simulated annealing method are given in Tab. 3 and 4. As seen from the tables, the function value can be reduced by 4–5 orders of magnitude after 70 iterations (about 1500 calculations of the objective function). The subsequent columns of the presented tables give the number of iterations (ITER), number of calculations of the objective function (NUM_F), search step value (STEP), value of the objective function (F) and values of the coordinates (X[I]).

Table 3. Searching for the extremum of the chained Rosenbrock function ($n = 10$) using the Hooke–Jeeves/simulated annealing method; $\tau = 6.0$, $\alpha = 0.8$.

ITER	NUM_F	STEP	F	X[1]	x[2]	X[3]	x[4]
1	0	0.300000E+001	0.205700E+004	−0.120000E+001	0.100000E+001	−0.120000E+001	0.100000E+001
10	188	0.177147E+001	0.193996E+003	0.987028E+000	0.999976E+000	0.871453E+000	0.999979E+000
35	713	0.141304E+000	0.151816E+002	0.987028E+000	0.988531E+000	0.871453E+000	0.815894E+000
60	1237	0.295804E−001	0.122840E+000	0.999171E+000	0.992068E+000	0.993329E+000	0.988676E+000
75	1552	0.609035E−002	0.483857E−002	0.999171E+000	0.997841E+000	0.998720E+000	0.996892E+000

ITER	x[5]	x[6]	x[7]	x[8]	x[9]	x[10]
1	−0.120000E+001	0.100000E+001	−0.120000E+001	0.100000E+001	−0.120000E+001	0.100000E+001
10	0.208529E+000	0.999984E+000	0.122995E+001	0.999978E+000	0.986969E+000	0.100000E+001
35	0.787436E+000	0.833896E+000	0.878168E+000	0.970435E+000	0.986969E+000	0.985869E+000
60	0.988156E+000	0.996041E+000	0.984503E+000	0.983983E+000	0.986053E+000	0.971663E+000
75	0.996244E+000	0.996041E+000	0.995242E+000	0.993156E+000	0.986053E+000	0.972361E+000

Table 4. Searching for the global extremum of the trigonometric function
($n = 10$) using the Hooke–Jeeves/simulated annealing method; $\tau = 6.0$, $\alpha = 0.8$.

ITER	NUM_F	STEP	F_X	x[1]	x[2]	x[3]	x[4]
1	0	0.600000E+001	0.740053E+001	−0.120000E+001	0.100000E+001	−0.120000E+001	0.100000E+001
10	188	0.540000E+001	0.310516E+001	0.226978E+001	0.100000E+001	0.215578E+001	0.100000E+001
30	604	0.478599E+000	0.108203E+000	0.127446E+001	0.100000E+001	0.630662E+000	0.100000E+001
50	1023	0.387665E+000	0.738571E−002	0.112427E+001	0.100000E+001	0.979560E+000	0.100000E+001
70	1442	0.500947E−001	0.750749E−003	0.102989E+001	0.100000E+001	0.994351E+000	0.100000E+001

ITER	x[5]	x[6]	x[7]	x[8]	x[9]	x[10]
1	−0.120000E+001	0.100000E+001	−0.120000E+001	0.100000E+001	−0.120000E+001	0.100000E+001
10	0.234294E+001	0.100000E+001	0.273660E+001	0.100000E+001	0.234294E+001	0.100000E+001
30	0.102192E+001	0.100000E+001	0.786208E+000	0.100000E+001	0.109860E+001	0.100000E+001
50	0.102192E+001	0.936665E+000	0.960347E+000	0.981458E+000	0.104491E+001	0.950793E+000
70	0.990998E+000	0.974841E+000	0.988051E+000	0.100929E+001	0.102744E+001	0.981724E+000

3. Multipoint optimization of 3D blading in an LP turbine stage group

The flow efficiency of a group of two LP exit stages of a 50 MW turbine operating over a wide range of load is increased by means of optimization of 3D blade stacking lines. A combination of linear and compound sweep and lean is added to the blade design to obtain new 3D stacking lines of stator blades.

Under nominal conditions the stage group operates at a pressure drop from 0.42 to 0.1 bar, that is at a pressure ratio $p_{ex}/p_{in} = 0.24$ and mass flow rate 37.8 kg/s. The expected pressure ratio variations are between 0.14 (high load) and 0.33 (low load). Since earlier papers [6, 7] show that the energy effects of blade sweep and lean (especially lean) depend on the turbine load, the concept of multipoint optimization is used.

The objective function was assumed as the weighted average of the enthalpy loss of the stage group (including the leaving energy) from three values of load. The loss at the nominal load forms 50% of the value of the objective function. The remaining 50% comes from the loss at a low load and high load, 25% each. The enthalpy losses were evaluated by means of CFD calculations of the flow domain in the solver FlowER. The penalty function was imposed on the mass flow rate if it is changed by more than ±0.5%, as compared to the original design.

There were 12 shape parameters (6 for each stage) as listed in Tab. 5. The optimization of the LP stage group was conducted using the genetic/simplex algorithm. 480 geometries were calculated (1440 calculations of the loss coefficient for three values of load). The comparison of a meridional view for the original and final geometry of the stage group is illustrated in Fig. 4. Changes of the optimized parameters are given in Tab. 5. It is shown that the effects of compound sweep and straight lean are prevailing for these LP stages. However, one can also remark that compound lean can be more effective for some HP stages [4, 7].
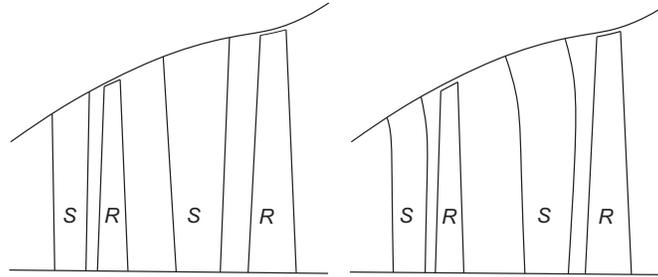
FIG. 4. Original (left) and final (right) geometry of the stage group in meridional view.

Table 5. Change of the optimized parameters in stages 1–2.

Optimized parameter	Its change	
	Stage 1	Stage 2
stator stagger angle[1] [°]	0.5	0.2
rotor stagger angle[1] [°]	0.2	−3.7
stator linear sweep angle[2] [°]	0.0	1.5
stator linear lean angle[3] [°]	−4.9	−6.4
stator compound sweep rate at tip[2] $\Delta x/l$ ($\Delta y = 3\Delta x$)	−0.08	−0.14
stator compound lean rate at root[3] $\Delta x/l$ ($\Delta y = 3\Delta x$)	0.00	−0.06

[1] positive value of stagger angle increment opens throats, negative value closes throats;

[2] positive value when the swept stator blade is protruded forward (downstream) at the tip;

[3] positive value when the leaned blade is protruded with rotation of the moving blades at the root.

The objective function was decreased by 1.8%. Most of efficiency gains come from optimization of the second (exit) stage. For example, the efficiency of the second stage for nominal operating conditions was increased by 2.4%, for low load even by as much as 5.5%. As a result of optimization, the stage group efficiency increases in the entire investigated range of load with the largest efficiency gains in the region of low and nominal load.

The comparison of Mach number contours at the root of the original and optimized second stage for a high load (exit volumetric flow rate of 800 m^3/s) is presented and in Fig. 5. Due to the low (negative) reaction of the original second stage at the exit, the stator is overloaded at the root, whereas the rotor remains underloaded there. High velocities downstream of the overloaded stator give rise to a shock wave configuration at the trailing edge and lead to inlet shock conditions for the rotor. The suction side boundary layer of the original rotor at the root section is thus affected by the inlet shock wave, resulting in a local adverse pressure gradient, which leads to the separation of the boundary layer with a quite large separation zone.

The optimized combination of stator blade sweep and lean leads to a reduction of the spanwise gradient of reaction, which in turn leads to a reduction of load of stator passages at the root and consequently, to a decrease of flow losses in the boundary layers, in the trailing edge and shock wave regions. This is also accompanied by a reduced risk of appearance of an inlet shock wave in the rotor. The load is increased in the rotor and the suction side boundary layer becomes regular with a moderate downstream pressure gradient and no suction side separation zone. A drawback is that the trailing edge velocities in the rotor are largely increased over the subsonic range, leading to a trailing edge shock wave configuration, which can also be observed from Mach number plots in Fig. 5.
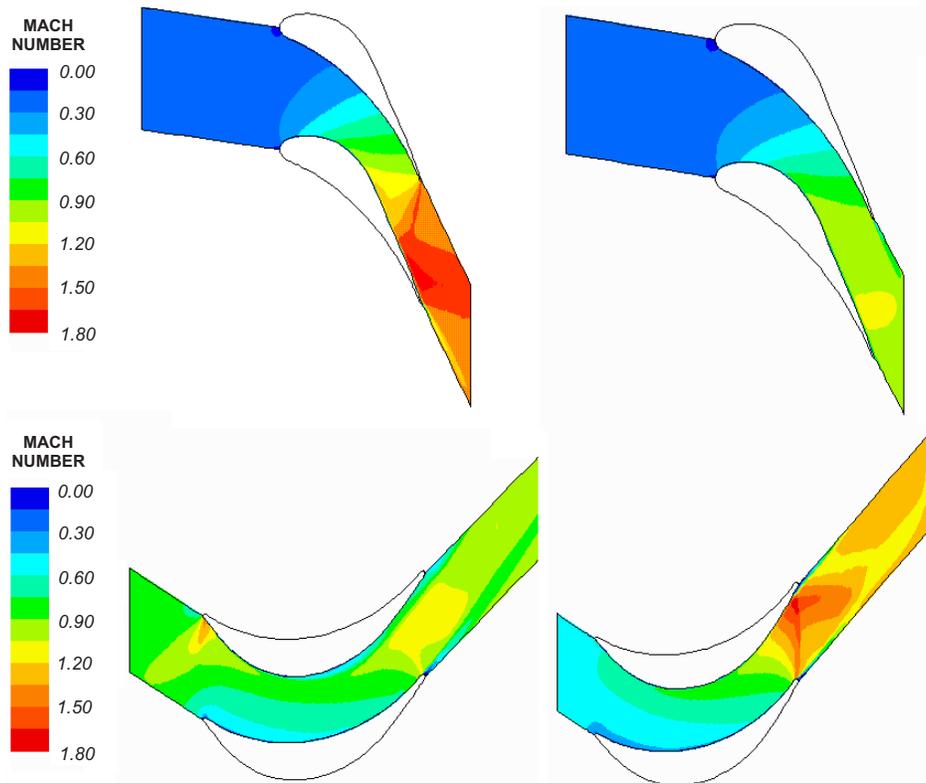
FIG. 5. Mach number contours in the second-stage stator (top) and rotor (bottom) at the root for original (left) and optimized (right) geometry for the exit volumetric flow rate of $800 \text{ m}^3/\text{s}$.

The comparison of entropy function contours at the exit from the upper part of the flow channel (tip region) in the second-stage rotor is presented in
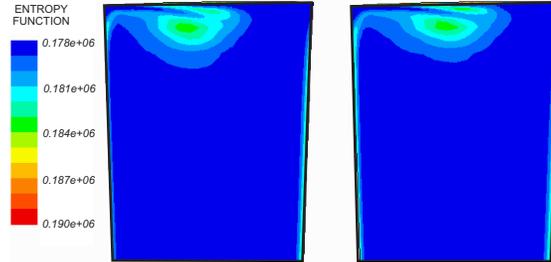
Fig. 6. Entropy function contours at the exit from the second-stage rotor in the tip region for original (left) and optimised (right) geometry for the exit volumetric flow rate of 520 m^3/s.

Fig. 6. The rotor blades are unloaded at the tip in the optimized design, which leads to a slight decrease of endwall and tip leakage losses, and provides more efficiency gains obtained from optimization. The colour plots were obtained from post-optimized fine-mesh calculations. These fine-mesh calculations are here to validate the results of optimization.

4. Optimization of blade profiles in a low-load HP turbine stage

Optimization of stator and rotor profiles (PLK and R2 profiles) is carried out for a low-reaction high-pressure (HP) stage of a 200 MW turbine. The considered turbine stage operates at a pressure drop from 42 to 38 bar (pressure ratio $p_{ex}/p_{in} = 0.9$) and at a mass flow rate 57 kg/s.

The stator and rotor profiles are described by a set of circle arcs. In the course of shape optimization there were 12 free parameters of profile arcs plus two stagger angles. The objective function was the enthalpy loss including the exit energy. The penalty was imposed on the changes of mass flow rate larger than ±0.5%, as compared to the original operating flow rate.

The optimization was conducted using the combination of the Hooke–Jeeves method and simulated annealing. There were over 600 calculations of the objective function. The shape of the original and modified (optimised) profiles is illustrated in Fig. 7. The stagger angles of the stator and rotor blades remain the same as in the original setup. Changes of the shape of the stator blade are very small, slightly increasing the profile camber, thus increasing the flow turning within the cascade. Changes in the rotor are more visible. The rotor profile becomes thicker.

The objective function was decreased by 0.8%, which seems to be quite a considerable improvement. Let us remind that typical efficiency gains achieved from 3D reblading in high and intermediate pressure turbine stages usually do not exceed 0.5% [4, 7, 10]. Mach number contours presented in Fig. 8 exhibit an im-
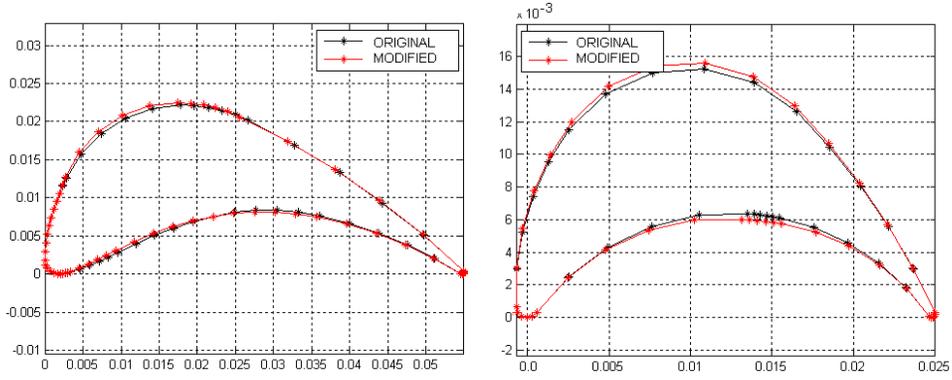
Fig. 7. Original and modified geometry of the stator (left) and rotor blades (right).
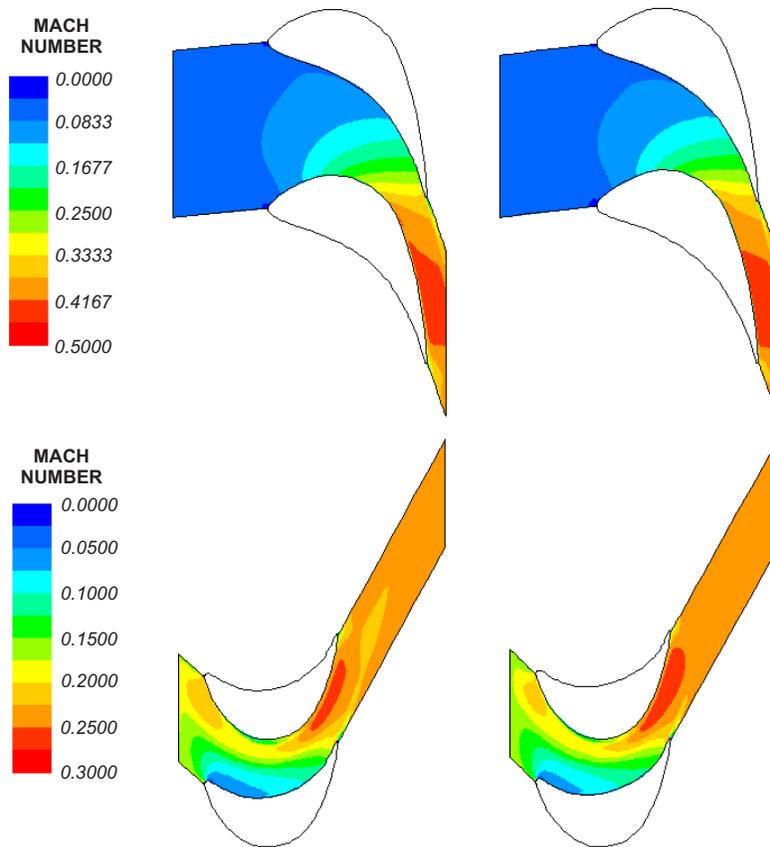
Fig. 8. Mach number contours in the stator (top) and rotor (bottom) at the mid-span: original geometry (left), modified geometry (right).

proved expansion in the modified rotor cascade. Total pressure contours shown
in Fig. 9 indicate a reduction in the intensity of endwall flows, especially in the
optimised rotor cascade, which becomes more aft-loaded. Thus, optimization of
the profile shape leads to the improvements both in a 2D and 3D flow through
the turbine cascades.
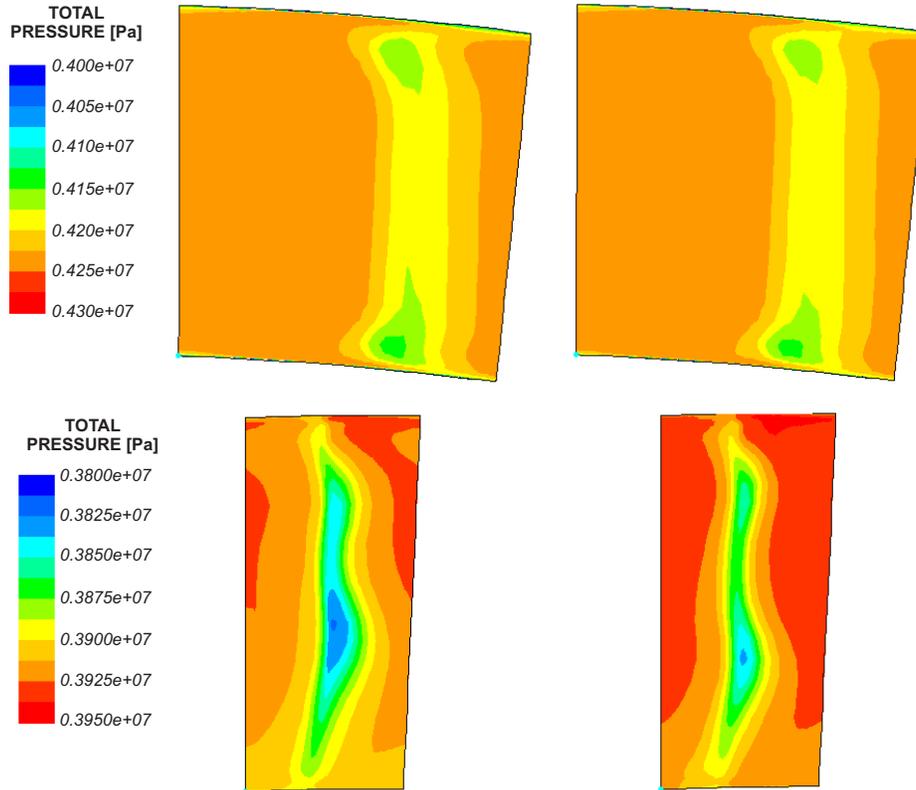
FIG. 9. Total pressure contours downstream of the stator (top) and rotor (bottom): original
geometry (left), modified geometry (right).

The stage mean reaction is increased by 3 %. Efficiency gains observed in
the flow-field contours can also be viewed from the spanwise distribution of
cascade and stage losses (stage losses are illustrated both without and with the
exit energy) presented in Fig. 10. As seen from this figure, stator losses are
slightly increased in the modified geometry (by 0.2% in the mean). However,
losses in the rotor are considerably lower (12% as compared to 13.9% in the
original geometry). Finally, stage losses are decreased both without the exit
energy (by 0.4%) and with the exit energy (by 0.8% from 10.4% down to 9.6%).
The assumed enthalpy loss definitions are gathered in the Appendix.
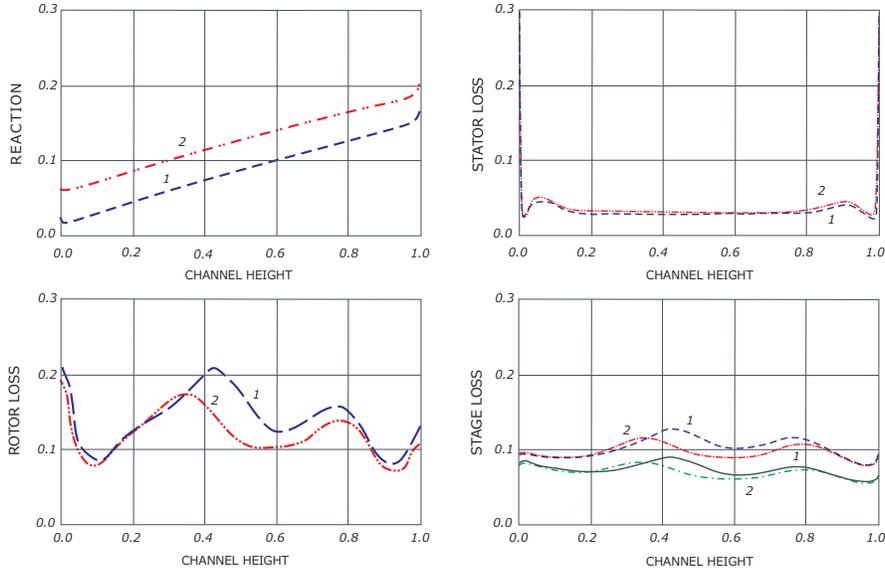
Fig. 10. Spanwise distribution of stage reaction (top left), stator losses (top right), rotor losses (bottom left) and stage loss with and without exit energy (bottom right) in an HP turbine stage: 1 – original geometry, 2 – modified geometry.

The CPU time needed for the optimization on a single processor Pentium 3GHz amounted to 4 days for the considered HP turbine stage and 2 weeks for the LP turbine stage group. Typically, just over 100 flow geometries were calculated each day. The computational time taken by the optimiser itself is negligible. The whole time needed for the optimization of the flow domain can be reduced by multi-processor flow calculations.

5. Conclusions

The paper describes the methods and results of direct constrained optimization of flow systems in the turbomachinery environment. Two new hybrid stochastic-deterministic methods are proposed. The first method is a combination of a genetic algorithm and simplex method of Nelder–Mead. The other method is a combination of a direct search method of Hooke–Jeeves and simulated annealing. Both methods were found to be effective in optimization of the chosen test functions (chained Rosenbrock and trigonometric function), usually decreasing the objective function at 8–10 dimensions by 4–5 orders of magnitude, with 1000–1500 calculations of the objective function.

Also two methods of parametrization of the blade profile are described. They make use of a set of circle arcs and rational Bezier functions. The methods al-

low parametrization of the blade profile using up to 10–25 parameters. 3D blade stacking lines are parametrized using linear and parabolic functions giving typically 10–15 free shape parameters. As a whole, the optimization system enables an efficient optimization of turbine blading systems, allowing us to tune a large number of geometrical parameters of the blade, including the blade number and stagger angle, stacking blade line parameters and blade section (profile) parameters.

The flow efficiency of a group of two LP exit stages of a 50 MW turbine operating over a wide range of load is increased by means of optimization of 3D blade stacking lines. Also low load profiles PLK-R2 were optimized for an HP turbine stage. The optimization of geometry of turbine blading systems can give considerable efficiency gains. It is found that optimization of 3D blade stacking lines in LP turbine stages can give over a 2% efficiency raise, especially thanks to the reduction of spanwise gradient of reaction, decreased flow losses in the boundary layers, separation zones, trailing edge and shock wave regions at the stator/rotor root. An up to 1% efficiency increase can easily be obtained from optimization of HP blade profiles and their restaggering, especially by making the rotor blade more aft-loaded and reducing the intensity of endwall flows.

Acknowledgements

Appendix

Definitions of stage reaction, enthalpy losses in the stator, rotor and stage (without or with the leaving energy) are gathered in Tab. 6 and are easily explained with the help of Fig. 11 – enthalpy-entropy graph for a turbine stage.

Table 6. Definition of reactions, cascade and stage losses.

| Stage reaction	$\rho = (h_1 - h_{2s})/(h_{0T} - h_{2s'})$
Enthalpy loss in stator	$\xi_1 = (h_1 - h_{1s})/(h_{0T} - h_{1s})$
Enthalpy loss in rotor	$\xi_2 = (h_2 - h_{2s})/(h_{1T} - h_{2s})$
Stage loss except exit energy	$\xi_{12} = (h_2 - h_{2s'})/(h_{0T} - h_{2s'})$
Stage loss with exit energy	$\xi_{12c} = (h_{2T} - h_{2s'})/(h_{0T} - h_{2s'})$
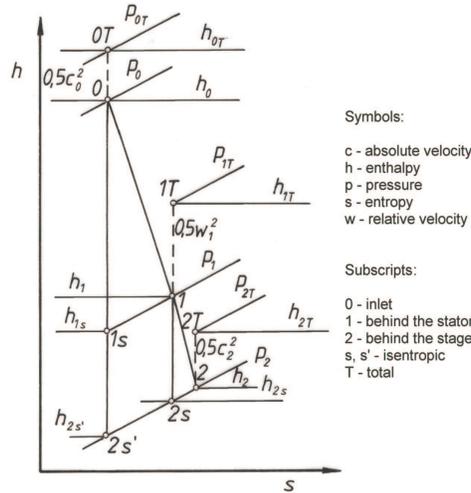
Fig. 11. Enthalpy-entropy graph for a turbine stage.

Compound sweep/lean displacements Δx, Δy for the stator blades are drawn in Fig. 12. The compound lean and sweep are assumed in a parabolic form. This picture can be considered either a meridional view of the compound swept stator blade or a circumferential view of the stator blade with compound lean.
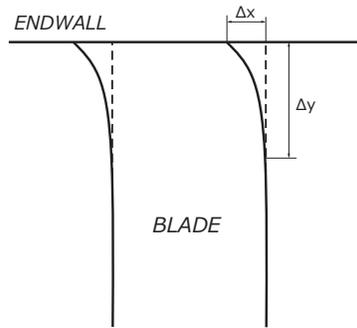

Fig. 12. Compound sweep/lean displacements.

References

1. J.D. Denton *Loss mechanisms in turbomachines*, ASME J. Turbomachinery, **115**, 621–656, 1993.

2. S. Harrison *The influence of blade lean on turbine losses*, ASME J. Turbomachinery, **114**, 184–190, 1992.

3. J.D. Denton, L. Xu, *The exploitation of 3D flow in turbomachinery design*, VKI LS, 1999-02, 1999.

4. P. Lampart, A. Gardzilewicz, *Numerical study of 3D blading in HP impulse turbines*, Cieplne Maszyny Przepływowe (Turbomachinery), **115**, 297–310, 1999.

5. A. Weiss, *Challenges in designing large low pressure steam turbines' final stages*, Proc. Conf. Modelling and Design in Fluid Flow Machinery, November 18–21, Gdańsk, Poland, pp. 183–191, 1977.

6. P. Lampart, S. Yershov, *Direct constrained CFD-based optimization of 3D blading for the exit stage of a large power steam turbine*, Trans. AMSE – J. Eng. Gas Turbines & Power, **125**, 1, 385–390, 2003.

7. P. Lampart, S. Yershov, A. Rusanov, *Increasing flow efficiency of high-pressure and low-pressure steam turbine stages from numerical optimization of 3D blading*, Engineering Optimization, **37**, 2, 145–166, 2005.

8. A. Demeulenaere, R. Van Den Braembussche, *Three-dimensional inverse method for turbomachinery blading design*, ASME J. Turbomachinery, **120**, 247–254, 1998.

9. G.S. Dulikravich, D.P. Baker, *Aerodynamic shape inverse design using a Fourier series method*, AIAA Paper 99-0185, 1999.

10. S. Pierret, R. Van Den Braembussche, *Turbo-machinery blade design using a Navier–Stokes solver and artificial neural network*, ASME Paper 98-GT-4, 1, 1998.

11. K. Kosowski, K. Tucki, A. Kosowski, *Turbine stage design aided by artificial intelligence methods*, Expert Syst. Appl., **36**, 9, 11536–11542, 2009.

12. V. Iliopoulou, I. Lepot, P. Geuzaine, *Design optimization of a HP compressor rotor blade and its hub endwall*, AMSE Pap. GT2008-50293, 2008.

13. A.I.J. Forrester, A. Sobester, A.J. Keane, *Engineering design via surrogate modeling: a practical guide*, Wiley, Chichester 2008.

14. A. Hedar, M. Fukushima, *Minimizing multimodal functions by simplex coding genetic algorithm*, Optimization Methods and Software, **18**, 265–282, 2003.

15. R. Chelouah, P. Siarry, *A hybrid method combining continuous tabu search and Nelder–Mead Simplex algorithms for the global optimization of multiminima functions*, Europ. J. Operational Research, **161**, 636–654, 2005.

16. P. Lampart, K. Augustyniewicz, *Hybrid stochastic-deterministic methods for optimization of flow systems*, Herald of Aeroengine Building, **3**, 22–26, 2007.

17. M.E. Dejcz, G.A. Filippov, L. Ja. Lazarev, *Atlas of axial turbine cascade profiles*, Maszinostrojenie, Moskwa 1965 [in Russian].

18. G. Farin, *Curves and surfaces for computer-aided geometric design*, Elsevier, Science & Technology Books, 1997.

19. S. Yershov, A. Rusanov, *The application package FlowER for the calculation of 3D viscous flows through multi-stage turbomachinery*, Certificate of state registration of copyright, Ukrainian state agency of copyright and related rights, February 19, 1996.

20. S. Yershov, A. Rusanov, A. Gardzilewicz, P. Lampart, J. Świrydczuk, *Numerical simulation of 3D flow in axial turbomachines*, TASK Quarterly, **2**, No. 2, 319–347, 1998.

21. F.R. Menter, *Two-equation eddy-viscosity turbulence models for engineering applications*, AIAA J., **32**, 8, 1598–1605, 1994.

22. J. Kaczorowski, *Strength analysis of marine propeller blade (theory and construction)*, Rep. CTO No. RK-87/R-125, 1987 [in Polish].

23. T. Tuszkowska-Koronowicz, *Adaptation of code WYKA for structure calculation for NBW*, Rep. IMP PAN 143/09, 2009 [in Polish].

24. P. Lampart, Ł. Hirt, A. Nastałek, K. Augustyniewicz, T. Tuszkowska-Koronowicz, *Increasing efficiency of turbine blading systems in supercritical power units with application of optimization methods*, Rep. IMPPAN No. 205/2009, presented at Conference: Supercritical Power Units, Szczyrk–Orle Gniazdo, April 22–23, 2009 [in Polish].

25. ANSYS, *ANSYS Fluent 12.0*, 2010.

26. P. Lampart, *Investigation of endwall flows and losses in axial turbines, Part I. Formation of endwall flows and losses*, J. Theoret. Appl. Mech., **47**, 2, 321–342, 2009.

27. B.E. Launder, G.J. Reece, W. Rodi, *Progress in the development of a Reynolds-stress turbulence closure*, J. Fluid Mechanics, **68**, Part 3, 537–566, 1975.

28. R. Langtry, F. Menter, *Transition Modeling for General CFD Applications in Aeronautics*, AIAA Paper 2005-522, 2005.

29. R. Hooke, T.A. Jeeves, *Direct search solution of numerical and statistical problems*, J. Assoc. Computing Machinery, **8**, No. 2, 212–229, 1961.

30. J.A. Nelder, R. Mead, *A simplex method for function minimization*, Computer Journal, **7**, No. 1, 308–313, 1965.

31. D.E. Goldberg, 1995, *Genetic algorithms and their applications*, WNT Warsaw 1995 [in Polish].

32. S. Kirkpatrick, C. Gelatt, M. Vecchi, *Optimization by simulated annealing*, Science, **4598**, 1983.

33. P.M. Pardalos, H.E. Romelin, *Handbook of global optimization, Vol.2, Nonconvex optimization and its application*, Kluwer Academic Publishers, Boston/Doordrecht/London 2002.